

Finite-volume effects on phase transition in the Polyakov-loop extended Nambu-Jona-Lasinio model with a chiral chemical potential

Zan Pan^{a,1,2}, Zhu-Fang Cui^{b,3}, Chao-Hsi Chang^{c,1,2,4}, Hong-Shi Zong^{d,1,3,5}

¹Key Laboratory of Theoretical Physics, Institute of Theoretical Physics, CAS, Beijing, 100190, China

²School of Physical Sciences, University of Chinese Academy of Sciences, Beijing 100049, China

³Department of Physics, Nanjing University, Nanjing 210093, China

⁴CCAST (World Laboratory), P.O. Box 8730, Beijing 100190, China

⁵Joint Center for Particle, Nuclear Physics and Cosmology, Nanjing 210093, China

Received: November 23, 2016

Abstract To investigate finite-volume effects on the chiral symmetry restoration and the deconfinement transition and some impacts of possible global topological background for a quantum chromodynamics (QCD) system with $N_f = 2$ (two quark flavors), we apply the Polyakov-loop extended Nambu-Jona-Lasinio model by introducing a chiral chemical potential μ_5 artificially. The final numerical results indicate that the introduced chiral chemical potential does not change the critical exponents but shifts the location of critical end point (CEP) significantly; the ratios for the chiral chemical potentials and temperatures at CEP, μ_c/μ_{5c} and T_c/T_{5c} , are significantly affected by the system size R . The behavior is that T_c increases slowly with μ_5 when R is ‘large’ and T_c decreases first and then increases with μ_5 when R is ‘small’. It is also found that for a fixed μ_5 , there is a R_{\min} , where the critical end point vanishes, and the whole phase diagram becomes a crossover when $R < R_{\min}$. Therefore, we suggest that for the heavy-ion collision experiments, which is to study the possible location of CEP, the finite-volume behavior should be taken into account.

Keywords PNJL model · QCD phase transitions · critical exponents · finite-volume effects

PACS 12.38.Aw, 12.38.Mh, 12.39.-x, 25.75.Nq

1 Introduction

The thermodynamics of strongly interacting matter ruled by quantum chromodynamics (QCD) under extreme conditions of temperature and density is a profound and challenging area overlapping statistical, particle and nuclear physics. A

deep understanding of its phase structure of QCD is expected to bring some insights on many fundamental problems such as compact stars, and the early universe [1, 2]. Experiments with heavy-ion collisions such as the BNL Relativistic Heavy-Ion Collider (RHIC) and the CERN Large Hadron Collider (LHC) are continuing active investigations on the strongly interacting matter in the laboratory [3, 4].

It is expected that QCD could lead to a rich phase structure of matter [5]. Lattice simulations from the first principle have revealed that the confined quarks will become released to quark-gluon plasma around the temperature $T_c = 154(9)$ MeV [6, 7]. However, due to the sign problem, Monte Carlo methods can be only directly applied to states around zero quark density. Therefore, effective models which exhibit the features of color confinement and spontaneous chiral symmetry breaking are more feasible to be used to study the phase structure of QCD on the density in addition to temperature. Here, we will adopt the Polyakov-loop extended Nambu-Jona-Lasinio (PNJL) model with chiral and axial chemical potentials [8–11].

In the PNJL model with some assumptions, it is found that the chiral symmetry restoration and deconfinement transition may coincide, i.e. discontinuities appear simultaneously in their order parameters, the chiral condensate σ and the Polyakov loop L , and they are of the first order [8–11]. A nontrivial critical end point (CEP) also exists at finite temperature T and a quark chemical potential μ , which indicates a coincidence of second-order phase transitions [8–11]. Although the axial currents are not conserved due the global topological solutions of QCD (such as instantons etc.) and quantum anomaly [12], to characterize imbalance on the chirality in terms of N_L and N_R ($N_R + N_L = N$, $N_R - N_L = N_5$) for the quark matter, we follow the authors of Ref. [12], similar to the chemical potential μ , introduce a chiral chemical potential μ_5 (conjugate to N_5) as a mathematical artifice to mimic the effects of ‘chiral transitions’. This also leads to

^ae-mail: panzan@itp.ac.cn

^be-mail: phycui@nju.edu.cn

^ce-mail: zhangzx@itp.ac.cn

^de-mail: zonghs@nju.edu.cn

a novel idea, proposed in Ref. [13], to detect the CEP by simulating QCD but with the chiral chemical potential μ_5 , then by continuation in the plane of $\mu_5 - \mu$, the critical end point CEP denoted by CEP_5 can be obtained, which is accessible to lattice QCD simulations of grand-canonical ensembles. Thus the authors of Ref. [13] believe that it should be a signal for the existence of the CEP in QCD if a CEP_5 is found by lattice simulation. Besides, since physical systems in the same universality class all share the same critical exponents, so here we would like to check if this continuation is reasonable by precise checking the impacts on the critical exponents brought by the introduction of μ_5 .

For the two-flavor PNJL model, there are unphysical decays of hadrons to quarks due to the spurious poles in the quark loop diagrams [14, 15]. Introducing a lower momentum cutoff to mimic confining effects of strong interaction helps to address this problem. This is also the starting point for us further to incorporate the finite-volume effects. In experiments of heavy-ion collisions, the strongly interacting matter formed through the energy deposition of the colliding particle definitely has a finite volume. Therefore, it is very important to have a knowledge on the finite-volume effects when studying the thermodynamic phases experimentally. In the context of heavy-ion collisions, the importance of finite-volume effects in the thermodynamics of strong interaction matter may be brought forward with the help of finite size scaling analysis [16, 17]. In the past years, many theoretical studies of finite-volume effects have been performed on NJL models [18–20]. However, only recently the studies on the thermodynamic properties of strongly interacting matter in a finite volume using the PNJL models have aroused increasing attention [21–23].

Our paper is organized as follows. First, in Sec. 2 we briefly review the PNJL model with chemical and chiral chemical potentials in the mean field approximation. In Sec. 3, numerical results on chiral symmetry restoration and deconfinement transition for $N_f = 2$ model with the infinite size are presented. We also verify that the chiral chemical potential does not impact on the value of critical exponents. By introducing the lower momentum cutoff, we investigate its finite-volume effects in Sec. 4. Finally, in Sec. 5 we summarize our results and some conclusions are made.

2 The PNJL model and its extension in mean field approximation

In this section, firstly we briefly review the PNJL model and its extension in the mean field approximation [9, 11]. The Lagrangian for PNJL model is given by

$$\mathcal{L} = \bar{\psi}(i\not{D} - m)\psi + G[(\bar{\psi}\psi)^2 + (i\bar{\psi}\gamma_5\tau\psi)^2] - \mathcal{U}(L, L^\dagger, T), \quad (1)$$

where $\psi = (u, d)$ represents the quark fields; so the number of flavors is taken as $N_f = 2$, and the number of colors is $N_c = 3$; the two-flavor current quark mass matrix is $m = \text{diag}(m_u, m_d)$, and we shall work in the isospin-symmetric limit with $m_u = m_d$; τ corresponds to the Pauli matrices in flavor space.

The potential term $\mathcal{U}(L, L^\dagger, T)$ is the effective potential expressed in terms of the traced Polyakov loop L and its conjugate

$$L = \frac{1}{N_c} \text{Tr}_c W, \quad L^\dagger = \frac{1}{N_c} \text{Tr}_c W^\dagger. \quad (2)$$

The Polyakov loop W is a matrix in color space explicitly given by

$$W = \mathcal{P} \exp \left[i \int_0^\beta A_4(\mathbf{x}, \tau) d\tau \right], \quad (3)$$

where $\beta = 1/T$ is the inverse temperature and $A_4 = iA^0$. In the Polyakov gauge, W can have a diagonal representation in color space [8]. The traced Polyakov loop L is an exact order parameter of spontaneous \mathbb{Z}_3 symmetry breaking in pure gauge theory. Although in full QCD the presence of dynamical quarks explicitly breaks the \mathbb{Z}_3 symmetry, it still seems to be a good indicator of the deconfinement phase transition. To incorporate the confinement or deconfinement properties, we have introduced a Polyakov-loop-dependent coupling constant G as

$$G = g[1 - \alpha_1 LL^\dagger - \alpha_2(L^3 + L^{\dagger 3})]. \quad (4)$$

For simplicity we will take $L = L^\dagger$ following Refs. [11, 13], which implies $A_4^8 = 0$. As shown in Ref. [24], the effects of fluctuations leading to $L \neq \bar{L}$ turn out not to be of major qualitative importance in determining the phase diagram. The numerical values of α_1 and α_2 can be obtained by a best fit of lattice data at zero and imaginary chemical potential, which leads to $\alpha_1 = \alpha_2 = 0.2$.

Now let us consider the extended PNJL model, since we would like to treat quark matter with chirality imbalance $N_5 = N_R - N_L$. The way to do it is, besides the chemical potential μ conjugated to the density n , additionally to introduce a chiral chemical potential μ_5 conjugated to the chiral density n_5 [13, 25, 26]. At Lagrangian level, this amounts to add the density operator $\mu \bar{\psi}\gamma^0\psi$ and the chiral density operator $\mu_5 \bar{\psi}\gamma^0\gamma^5\psi$ to Eq. (1). Namely the Lagrangian (1) for the model has been extended to the following

$$\mathcal{L} = \bar{\psi}(i\not{D} - m + \mu\gamma^0 + \mu_5\gamma^0\gamma^5)\psi + G[(\bar{\psi}\psi)^2 + (i\bar{\psi}\gamma_5\tau\psi)^2] - \mathcal{U}(L, L^\dagger, T). \quad (5)$$

Making the mean field approximation and performing the path integral over the quark field, we can obtain the ther-

modynamic potential density \mathcal{V} at the one-loop level

$$\begin{aligned} \mathcal{V} = & \mathcal{U}(L, L^\dagger, T) + G\sigma^2 - N_c N_f \sum_{s=\pm 1} \int \frac{d^3\mathbf{p}}{(2\pi)^3} \omega_s \\ & - N_f \sum_{s=\pm 1} \int \frac{d^3\mathbf{p}}{(2\pi)^3} T \log(F_+ F_-), \end{aligned} \quad (6)$$

where $\sigma = \langle \bar{\psi}\psi \rangle$ is the chiral condensate and relates to the effective quark mass M as

$$M = m - 2G\sigma. \quad (7)$$

The index s denotes the helicity projection and

$$\omega_s = \sqrt{(|\mathbf{p}|s - \mu_s)^2 + M^2} \quad (8)$$

corresponds to the pole of the quark propagator. The momentum integral for ω_s corresponds to the vacuum quark fluctuations and a momentum cutoff Λ is introduced to regularize it here.

The last term in Eq. (6) is responsible for the statistical properties of the model at low temperature. Therein we have introduced the functions

$$\begin{aligned} F_- &= 1 + 3Le^{-\beta(\omega_s - \mu)} + 3L^\dagger e^{-2\beta(\omega_s - \mu)} + e^{-3\beta(\omega_s - \mu)}, \\ F_+ &= 1 + 3L^\dagger e^{-\beta(\omega_s + \mu)} + 3Le^{-2\beta(\omega_s + \mu)} + e^{-3\beta(\omega_s + \mu)}. \end{aligned} \quad (9)$$

In order to reproduce the pure gluonic lattice data with $N_c = 3$, the potential term \mathcal{U} is taken as the following form

$$\begin{aligned} \mathcal{U}(L, L^\dagger, T) = & T^4 \left\{ -\frac{1}{2}a(T)LL^\dagger + b(T) \ln [1 - 6LL^\dagger \right. \\ & \left. + 4(L^3 + L^{\dagger 3}) - 3(LL^\dagger)^2] \right\}, \end{aligned} \quad (10)$$

where the model parameters are given by

$$a(T) = a_0 + a_1 \left(\frac{T_0}{T}\right) + a_2 \left(\frac{T_0}{T}\right)^2, \quad (11)$$

$$b(T) = b_3 \left(\frac{T_0}{T}\right)^3. \quad (12)$$

The choice of coefficients from the mean field approximation reads

$$a_0 = 3.51, \quad a_1 = -2.47, \quad a_2 = 15.2, \quad b_3 = -1.75. \quad (13)$$

Other numerical parameters used in our calculations are taken as those in Ref. [11]

$$\begin{aligned} T_0 &= 190 \text{ MeV}, \quad \Lambda = 631.5 \text{ MeV}, \\ m &= 5.5 \text{ MeV}, \quad g = 5.498 \times 10^{-6} \text{ MeV}^{-2}. \end{aligned} \quad (14)$$

3 Chiral symmetry restoration and deconfinement transition in the extended PNJL model

In this section we will present the way to find chiral symmetry restoration and deconfinement transition in the PNJL model with chemical potential μ and chiral chemical potential μ_5 , and show its reasonableness for investigating the QCD phase transitions.

For any given μ , μ_5 and T , we can obtain the corresponding values of σ and L by solving the gap equations

$$\frac{\partial \mathcal{V}}{\partial \sigma} = 0, \quad \frac{\partial \mathcal{V}}{\partial L} = 0. \quad (15)$$

However, this approach is hard to work in practice due to the difficulty in solving the coupled integral equations by means of iterative methods. Moreover, the solutions of these equations do not necessarily yield a global minimum. There are possibilities that they may yield a local minimum, even a maximum. Therefore here not only to find the solutions of Eq. (15) we also need to check that the corresponding solution yields a global minimum when they are inserted back into Eq. (6). For a better approach, we can solve the problem in another way, i.e. to solve Eq. (15) by finding the minima of the potential function \mathcal{V} . This reduces to the famous problem of multidimensional minimization, and here we can use the efficient Nelder-Mead simplex algorithm.

First, we consider the case when $\mu_5 = 0$. For any given μ and T , we can calculate the solutions of Eq. (15). As shown in Fig. 1, the discontinuity of the effective mass M and that of the Polyakov loop L vanish simultaneously at the same point, that determines the CEP as $(\mu_c, T_c) = (172.7, 159.2)$. Our numerical calculation here for the critical temperature is in good agreement with the result $T_c = 154(9)$ MeV obtained by lattice QCD [6]. There is a long-standing debate, whether the chiral symmetry restoration and the deconfinement transition have a correspondence or not [27], whereas in our PNJL model the two phase transitions coincide exactly and both are of first-order transitions.

For $\mu = 0$, we can also determine the location of CEP₅: $(\mu_{5c}, T_{5c}) = (307.6, 166.1)$, which is plotted in Fig. 2. It is interesting that the critical temperature is almost unchanged in the continuation of CEP to CEP₅. In Ref. [13], a novel idea on location of the CEP has been suggested by using the relations μ_c/μ_{5c} . Namely when lattice simulations find CEP₅, then it indicates a signal for the existence of the CEP in QCD.

As linear response of the physical system to some external field, susceptibilities are widely used to study the phase transitions of strongly interacting matter [28]. Here, let us consider three kinds of susceptibilities: the vector susceptibility χ_v , the axial-vector susceptibility χ_{av} , and the thermal

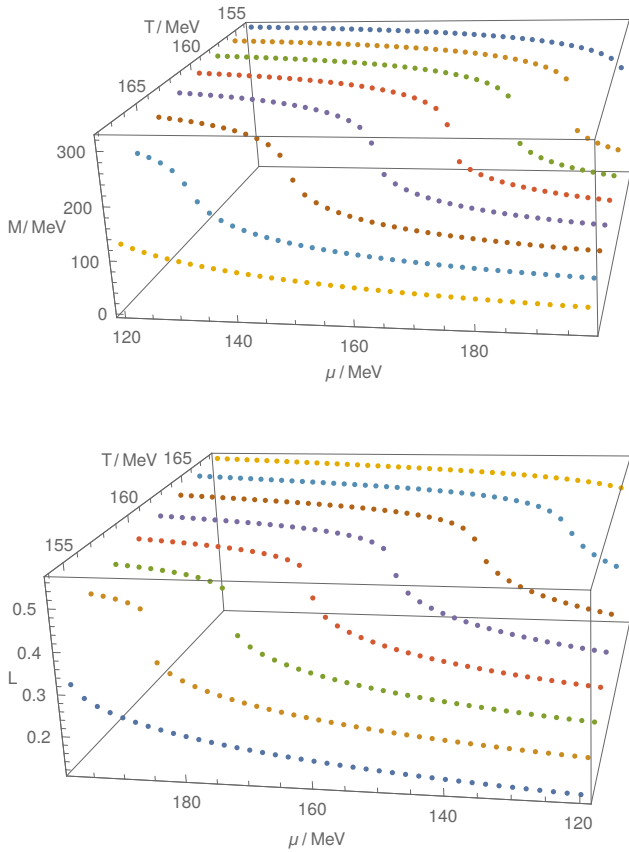


Fig. 1 3D plot for the effective mass M (upper panel) in the μ - T - M space and the Polyakov loop L (lower panel) in the μ - T - L space near the CEP $(\mu_c, T_c) = (172.7, 159.2)$, where $\mu_5 = 0$.

susceptibility χ_T . They are defined as follows

$$\chi_v = \frac{\partial \sigma}{\partial \mu}, \quad \chi_{av} = \frac{\partial \sigma}{\partial \mu_5}, \quad \chi_T = \frac{\partial \sigma}{\partial T}. \quad (16)$$

All these susceptibilities are singular at the CEP or CEP₅ and are continuous in the crossover region, so we may use this fact to accurately identify the location of CEP and/or CEP₅.

As well-known, a susceptibility in the vicinity of CEP or CEP₅ diverges in a power law with the so-called critical exponent γ . These exponents are only dependent on the dimension of space and the order parameter(s), but do not involve the details of microscopic dynamics. Different systems in the same universality class all will share the same critical behavior. Practically and for simplicity, we may choose a specific direction, which is denoted by “ \rightarrow ”, to calculate the critical exponents by the path from lower μ or μ_5 toward higher μ_c or μ_{5c} with the temperature $T = T_c$ being fixed. Using the linear logarithm fit, we obtain

$$\log \chi = -\gamma \log |T - T_c| + \text{const}. \quad (17)$$

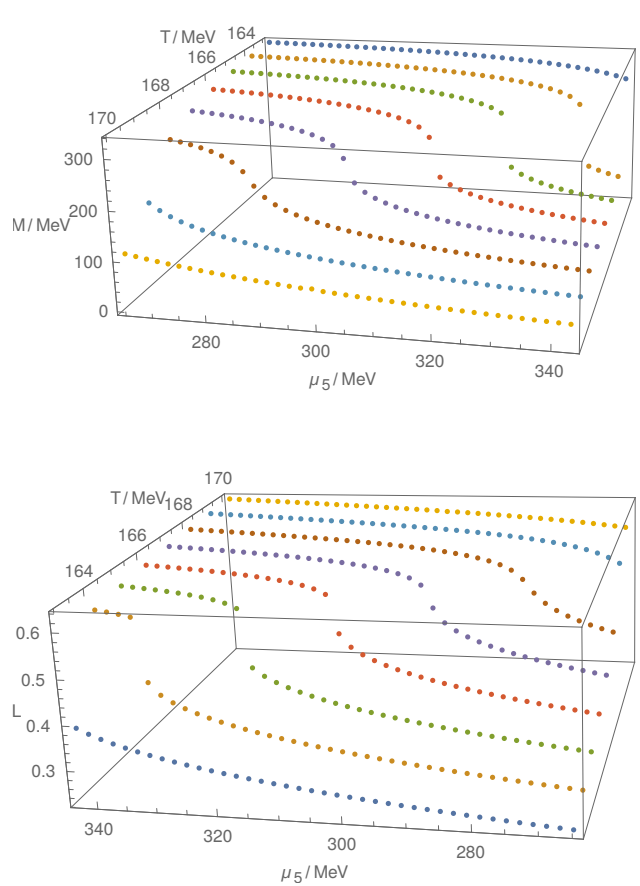


Fig. 2 The 3D plot for the effective mass M in μ_5 - T - M space (the upper one) and the (3D) plot for the Polyakov loop L in μ_5 - T - L space (the lower one) near the CEP₅ $(\mu_{5c}, T_{5c}) = (307.6, 166.1)$, where $\mu = 0$.

The critical exponent of the vector-scalar susceptibility in the direction “ \rightarrow ” is calculated in Fig. 3.

Similarly, as necessary checks, we also calculate the critical exponent in the other directions such as those denoted as “ \leftarrow ”, “ \uparrow ”, “ \downarrow ” with the path from higher μ or μ_5 toward μ_c or μ_{5c} , the path from lower T toward T_c , and the path from higher T toward T_c respectively. The critical exponents of χ_v and χ_T in these four directions for $\mu_5 = 0$ are calculated and put in Table 1; the critical exponents of χ_{av} and χ_T for $\mu = 0$ are also calculated and put in Table 2. The obtained critical exponents all agree with the predictions about the universality by mean field method [29, 30], and in Ref. [31], more critical exponents are calculated in the NJL model.

For $\mu_5 \neq 0$ and $\mu \neq 0$, CEP will naturally evolve into CEP₅. The discontinuity of the effective mass and Polyakov loop parameter vanishes at the same CEP, which means that the chiral symmetry restoration and the deconfinement transition coincide exactly. The projection of the evolution of CEP onto the μ - μ_5 plane is illustrated in Fig. 4, which also presents the results are in good agreement with the results

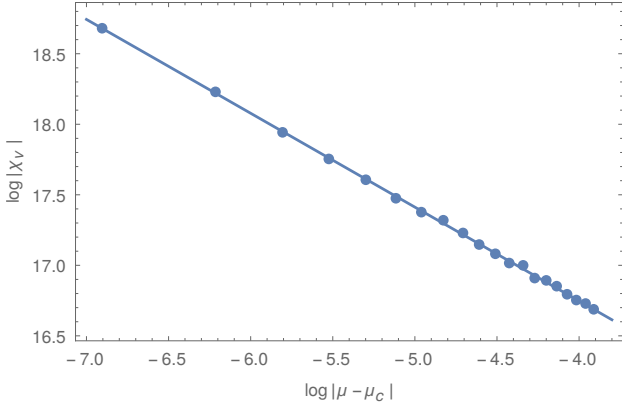


Fig. 3 The linear fit with the logarithm of the vector-scalar susceptibility χ_v as a function of $\log|\mu - \mu_c|$ at the fixed temperature T_c in the direction \rightarrow , where $\mu_5 = 0$. The critical exponent γ_v is calculated from the slope as 0.665 ± 0.030 .

Table 1 Critical exponents for $\mu_5 = 0$, where the CEP is calculated as $(\mu_c, T_c) = (172.7, 159.2)$.

Critical exponent	Path	Numerical result	MF exponent
γ_v	\rightarrow	0.665 ± 0.030	$\frac{2}{3}$
	\leftarrow	0.636 ± 0.059	
	\uparrow	0.679 ± 0.061	
	\downarrow	0.659 ± 0.085	
γ_T	\rightarrow	0.658 ± 0.014	$\frac{2}{3}$
	\leftarrow	0.664 ± 0.010	
	\uparrow	0.671 ± 0.012	
	\downarrow	0.664 ± 0.017	

Table 2 Critical exponents for $\mu = 0$, where the CEP₅ is calculated as $(\mu_{5c}, T_{5c}) = (307.6, 166.1)$.

Critical exponent	Path	Numerical result	MF exponent
γ_{av}	\rightarrow	0.697 ± 0.068	$\frac{2}{3}$
	\leftarrow	0.717 ± 0.082	
	\uparrow	0.694 ± 0.155	
	\downarrow	0.690 ± 0.172	
γ_T	\rightarrow	0.668 ± 0.042	$\frac{2}{3}$
	\leftarrow	0.728 ± 0.061	
	\uparrow	0.684 ± 0.013	
	\downarrow	0.671 ± 0.016	

in Ref. [13]. Furthermore, we verify that the nonzero chiral chemical potential does not change the critical exponents, and that γ_v , γ_{av} and γ_T are all approximately equal to $2/3$. This implies that for the QCD phase diagram our continuation of the CEP to a fictitious CEP belonging to a phase diagram in the μ_5 - T plane is reasonable.

4 The finite-volume effects for CEP and CEP₅

Since the strongly interacting matter formed through the energy deposition of colliding particles definitely has a finite volume, it is very important to have a clear understanding

of the finite-volume effects to fully contemplate the thermodynamic phases, which may be created in the experiments. In Refs. [23, 32], the variations of susceptibilities with temperature for different system sizes have been discussed, but here we would like to focus on the finite-volume effects regarding the CEP and CEP₅.

To incorporate the finite-volume effects, methods such as the Monte Carlo simulation [21] and the renormalization group approach [33] may work, but we will make a lower momentum cutoff $\lambda = \pi/R$ on the integration of the thermodynamic potential density \mathcal{V} of the extended PNJL model, where R is the size of the concerned system with a volume $\sim R^3$. Thus the thermodynamic potential density Eq. (6) is rewritten as

$$\mathcal{V} = \mathcal{U}(L, L^\dagger, T) + G\sigma^2 - N_c N_f \sum_{s=\pm 1} \int_{\lambda}^{\Lambda} \frac{d^3\mathbf{p}}{(2\pi)^3} \omega_s - N_f \sum_{s=\pm 1} \int_{\lambda}^{\infty} \frac{d^3\mathbf{p}}{(2\pi)^3} T \log(F_+ F_-), \quad (18)$$

here, several simplifications are made. The most important one is the infinite sum of Fourier series is replaced by an integration over a continuous variation of momentum with the lower cutoff. We also neglect the surface and curvature effects, and the slight changes due to introducing the lower cutoff for the other parameters, such as σ and the relevant ones in $\mathcal{U}(L, L^\dagger, T)$. The same simplifications to consider the finite-volume effects can also be found in Ref. [22, 23]. Obviously, when $\lambda = 0$ is taken (corresponding to $R = \infty$) in Eq. (18), all reduces to the case of infinite volume.

Following the same procedure as that in the previous section, we find the location of CEP or CEP₅ for various system sizes, and calculate out the corresponding critical exponents, and it has been found that the system size R does not affect the critical exponents. In Fig. 4, we plot the projection of the evolution of CEP to CEP₅ on the μ - μ_5 plane for various system sizes: $R = \infty$, 4 fm and 3 fm respectively. One can see clearly that the finite-volume effects become more and more manifest as R decreases, and are more important for lower μ_5 . We have also found that the CEP vanishes at a R_{\min} , whose precise value is estimated to be about 2.1 fm. Namely when $R < R_{\min}$, the whole phase diagram becomes a crossover. Our numerical results in Table 3 also show that the ratios μ_c/μ_{5c} and T_c/T_{5c} are significantly affected by system sizes. If we use the idea proposed in Ref. [13] to find the location of CEP, the finite-volume effects on these ratios should be taken into account.

In Fig. 5, we plot the projection of the evolution of CEP on the μ_5 - T plane for different system sizes. From the plot one can see that the relations between T_c and μ_5 are intriguing: when R is large, T_c increases slowly with μ_5 ; when R is small, T_c decreases first and then increases with μ_5 . In the case of large volumes, our results are qualitatively consistent

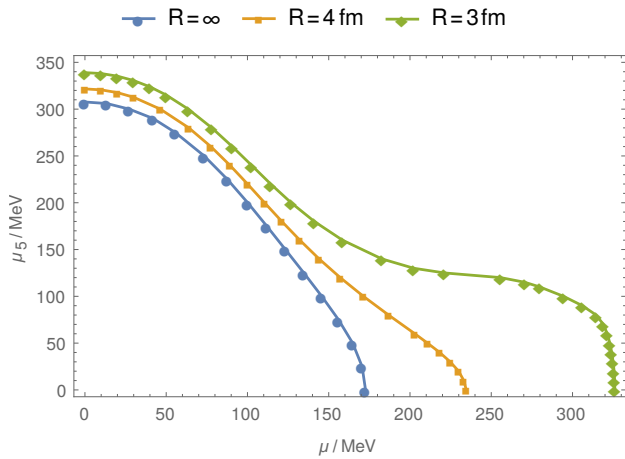


Fig. 4 Projection of the evolution of CEP on the μ - μ_5 plane for different system sizes: $R = \infty$, 4 fm, and 3 fm.

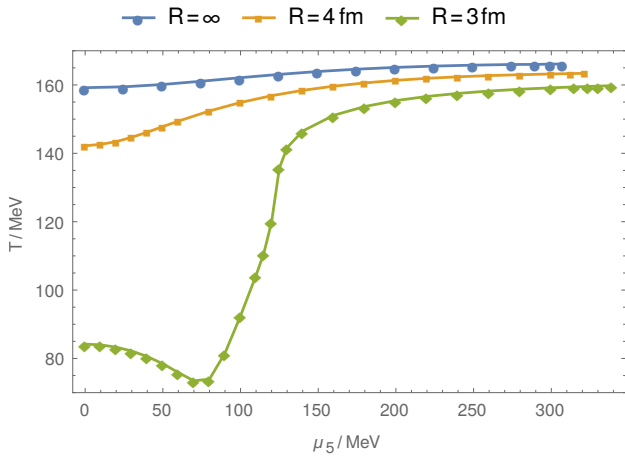


Fig. 5 Projection of the evolution of CEP on the μ_5 - T plane for different system sizes: $R = \infty$, 4 fm, and 3 fm.

Table 3 Numerical relations between CEP and CEP₅ for different system sizes.

R	(μ_c, T_c)	(μ_{5c}, T_{5c})	$(\mu_c / \mu_{5c}, T_c / T_{5c})$
∞	(172.7, 159.2)	(307.6, 166.1)	(0.561, 0.958)
5 fm	(194.5, 153.6)	(314.9, 164.7)	(0.618, 0.933)
4 fm	(234.6, 142.2)	(321.6, 163.4)	(0.729, 0.870)
3 fm	(326.0, 84.2)	(339.0, 159.8)	(0.962, 0.527)

with the results obtained within the framework of Dyson-Schwinger equations [34] and the lattice simulation [35]. However, we should point out that the other studies with different models or methods [25, 26, 36, 37] may have given opposite results in T_c decreasing with μ_5 . Whereas our calculations show that the dependence of T_c on μ_5 is changed by the system sizes, which means the finite-volume effects are very important in studying the phase transitions of effective models in QCD.

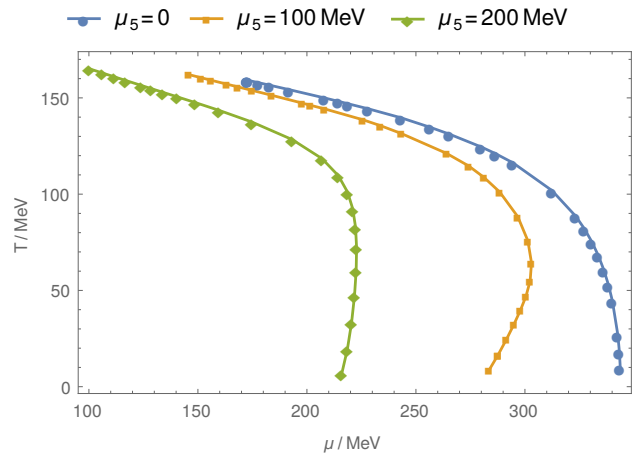


Fig. 6 Projection of the evolution of CEP on the μ - T plane for fixed chiral chemical potential: $\mu_5 = 0$, 100 MeV, and 200 MeV respectively, varying in the system sizes from $R = \infty$ with the highest critical temperature to R_{\min} with the lowest critical temperature. The corresponding values of R_{\min} are estimated around 2.1 fm, 2.0 fm, and 1.6 fm respectively.

Another interest point is to see the shift of CEP in the phase diagram with respect to the system size. In Fig. 6, we plot the projection of the evolution of CEP on the μ - T plane for fixed chiral chemical potential: $\mu_5 = 0$, 100 MeV, and 200 MeV respectively, varying the system sizes from $R = \infty$ with the highest critical temperature to R_{\min} with the lowest critical temperature. The corresponding values of R_{\min} are estimated around 2.1 fm, 2.0 fm, and 1.6 fm respectively. It is interesting to note that the relation between critical temperature and the system size may be nonmonotonic for some values of the chiral chemical potential such as $\mu_5 = 200$ MeV.

Our results on the finite-volume effects have significant implications for heavy-ion collision experiments, because the strong interacting matter formed in a heavy-ion collision is finite in volume, and its size depends on the size of the colliding nuclei, the collision center of mass energy \sqrt{s} , and the centrality of the collision. In our concerned case, \sqrt{s} and the centrality of collisions relate to the temperature T and the chiral chemical potential μ_5 when the colliding nuclei are chosen. It is expected that our results will provide some guidance for the experiments aiming at the search of the possible critical end point. Although there have been many efforts to estimate the size of the strong interacting matter formed by heavy-ion collisions [38–41], no general consensus have been reached. In Ref. [42], the system volume for Pb-Pb collisions with \sqrt{s} in the range of 62.4 to 2760 GeV has been estimated in the range to vary from 50 to 250 fm³, corresponding to a system size from 3 to 6 fm. Given that these are the volumes at the time of freeze out, one may expect an even smaller system size at the initial equilibration time [40, 41]. Note that our estimate adopts several approximations, then to test of our numerical results, possible uncertainties should be taken into account.

5 Summary and Conclusion

To summarize, we have studied the chiral symmetry restoration and the deconfinement transition of the phase diagram of QCD by using the extended PNJL model in which chemical and chiral chemical potentials μ and μ_5 are introduced. Our results show that the discontinuity of the effective mass and Polyakov loop parameter always vanishes at the same CEP, and the chiral symmetry restoration and the deconfinement, the two transitions, coincide exactly. Three kinds of susceptibilities are defined and the corresponding critical exponents are calculated. All the critical exponents are approximately equal to $2/3$. We also show that the critical exponents do not change even artificially introducing a chiral chemical potential μ_5 . This implies that the continuation for CEP of the QCD phase diagram to a fictitious CEP belonging to a phase diagram in the μ_5 - T plane is also meaningful.

Finally, it is found that the finite-volume effects become more and more manifest as R , the radius of the size for the considered finite-volume, decreases and are more important for a smaller μ_5 , by introducing a lower momentum cutoff in the integration in \mathcal{V} as Eq. (18) to investigate the finite-volume effects in the PNJL model. Numerical results show that the ratios μ_c/μ_{5c} and T_c/T_{5c} are significantly affected by the system sizes with radius R . When R is comparatively large, T_c increases slowly with μ_5 ; when R is comparatively small, T_c decreases first and then increases with μ_5 . For a fixed μ_5 , we can also determine a R_{\min} such that the CEP vanishes when $R < R_{\min}$, and the whole phase diagram becomes a crossover. The corresponding values of R_{\min} for $\mu_5 = 0, 100\text{MeV}$ and 200MeV are estimated around 2.1 fm , 2.0 fm and 1.6 fm respectively. Therefore, the present results on the finite-volume effects indicate that when investigating the CEP of QCD phases experimentally, the volume of strong interacting matter in the heavy-ion collision cannot be small, otherwise the result on CEP would be flexible.

Acknowledgements This work is supported in part by the National Natural Science Foundation of China under the Grants No. 11275243, No. 11535002, No. 11447601, No. 11275097, No. 11475085 and No. 11535005, the China Postdoctoral Science Foundation under the Grant No. 2015M581765, and the Jiangsu Planned Projects for Postdoctoral Research Funds under the Grant No. 1402006C.

References

1. K. Rajagopal, F. Wilczek, in *At the Frontier of Particle Physics: Handbook of QCD*, Vol. 3, edited by M. Shifman (World Scientific, 2001) pp. 2061–2151.
2. H. Satz, *Extreme States of Matter in Strong Interaction Physics*, Lecture Notes in Physics, Vol. 841 (Springer Berlin Heidelberg, 2012).
3. L. Adamczyk *et al.* (STAR Collaboration), *Phys. Rev. Lett.* **112**, 032302 (2014).
4. B. Abelev *et al.*, *Phys. Lett. B* **739**, 139 (2014).
5. K. Fukushima, T. Hatsuda, *Rep. Prog. Phys.* **74**, 014001 (2011).
6. A. Bazavov *et al.* (HotQCD Collaboration), *Phys. Rev. D* **85**, 054503 (2012).
7. P. Petreczky, *J. Phys. G* **39**, 093002 (2012).
8. K. Fukushima, *Phys. Lett. B* **591**, 277 (2004).
9. C. Ratti, M.A. Thaler, W. Weise, *Phys. Rev. D* **73**, 014019 (2006).
10. Y. Sakai, T. Sasaki, H. Kouno, M. Yahiro, *Phys. Rev. D* **82**, 076003 (2010).
11. R. Gatto, M. Ruggieri, *Phys. Rev. D* **85**, 054013 (2012).
12. K. Fukushima, D.E. Kharzeev, H.J. Warringa, *Phys. Rev. D* **78**, 074033 (2008).
13. M. Ruggieri, *Phys. Rev. D* **84**, 014011 (2011).
14. H. Hansen, W.M. Alberico, A. Beraudo, A. Molinari, M. Nardi, C. Ratti, *Phys. Rev. D* **75**, 065004 (2007).
15. D. Blaschke, A. Dubinin, M. Buballa, *Phys. Rev. D* **91**, 125040 (2015).
16. L.F. Palhares, E.S. Fraga, T. Kodama, *J. Phys. G* **38**, 085101 (2011).
17. E.S. Fraga, L.F. Palhares, P. Sorensen, *Phys. Rev. C* **84**, 011903 (2011).
18. L. Abreu, M. Gomes, A. da Silva, *Phys. Lett. B* **642**, 551 (2006).
19. S. Yasui and A. Hosaka, *Phys. Rev. D* **74**, 054036 (2006).
20. L.M. Abreu, A.P.C. Malbouisson, J.M.C. Malbouisson, *Phys. Rev. D* **83**, 025001 (2011).
21. M. Cristoforetti, T. Hell, B. Klein, W. Weise, *Phys. Rev. D* **81**, 114017 (2010).
22. A. Bhattacharyya, P. Deb, S.K. Ghosh, R. Ray, S. Sur, *Phys. Rev. D* **87**, 054009 (2013).
23. A. Bhattacharyya, R. Ray, S. Sur, *Phys. Rev. D* **91**, 051501 (2015).
24. S. Rößner, T. Hell, C. Ratti, W. Weise, *Ref. Nucl. Phys. A* **814**, 118 (2008).
25. K. Fukushima, M. Ruggieri, R. Gatto, *Phys. Rev. D* **81**, 114031 (2010).
26. M.N. Cherdub, A.S. Nedelin, *Phys. Rev. D* **83**, 105008 (2011).
27. S. Borsányi *et al.* (Wuppertal-Budapest Collaboration), *JHEP* **09**, 073 (2010).
28. Z.-F. Cui, F.-Y. Hou, Y.-M. Shi, Y.-L. Wang, H.-S. Zong, *Ann. Phys.* **358**, 172 (2015).
29. Y. Hatta, T. Ikeda, *Phys. Rev. D* **67**, 014028 (2003).
30. P. Costa, M.C. Ruivo, C.A. de Sousa, *Phys. Rev. D* **77**, 096001 (2008).
31. Y. Lu, Y.-L. Du, Z.-F. Cui, H.-S. Zong, *Eur. Phys. J. C* **75**, 495 (2015).
32. A. Bhattacharyya, R. Ray, S. Samanta, S. Sur, *Phys. Rev. C* **91**, 041901 (2015).

-
33. R.-A. Tripolt, J. Braun, B. Klein, B.-J. Schaefer, [Phys. Rev. D **90**, 054012 \(2014\)](#).
 34. S.-S. Xu, Z.-F. Cui, B. Wang, Y.-M. Shi, Y.-C. Yang, H.-S. Zong, [Phys. Rev. D **91**, 056003 \(2015\)](#).
 35. V.V. Braguta, E.-M. Ilgenfritz, A.Y. Kotov, B. Petersson, S.A. Skinderev, [Phys. Rev. D **93**, 034509 \(2016\)](#).
 36. J. Chao, P. Chu, M. Huang, [Phys. Rev. D **88**, 054009 \(2013\)](#).
 37. P.V. Buividovich, [Phys. Rev. D **90**, 125025 \(2014\)](#).
 38. M. Habich, J.L. Nagle, P. Romatschke, [Eur. Phys. J. C **75**, 1 \(2015\)](#).
 39. Y. Hirono, E. Shuryak, [Phys. Rev. C **91**, 054915 \(2015\)](#).
 40. P. Bożek, W. Broniowski, [Phys. Lett. B **720**, 250 \(2013\)](#).
 41. A. Bzdak, B. Schenke, P. Tribedy, R. Venugopalan, [Phys. Rev. C **87**, 064906 \(2013\)](#).
 42. G. Gräf, M. Bleicher, Q. Li, [Phys. Rev. C **85**, 044901 \(2012\)](#).